Integration of Type II Nanorod Heterostructures into Photovoltaics

Hunter McDaniel,[†,*] Philip Edward Heil,[†] Cheng-Lin Tsai,[†] Kyekyoon (Kevin) Kim,[‡] and Moonsub Shim[†,*]

[†]Department of Materials Science and Engineering, University of Illinois, Urbana, Illinois 61801, United States, and [‡]Department of Electrical and Computer Engineering, University of Illinois, Urbana, Illinois 61801, United States

ABSTRACT High-quality epitaxial interfaces and delicate control over shape anisotropy make nanorod heterostructures (NRHs) with staggered band offsets efficient in separating and directing photogenerated carriers. Combined with versatile and scalable wet chemical means of synthesis, these salient features of NRHs are useful for improving both the performance and the cost-effectiveness of photovoltaics (PVs). However, inefficient carrier transport and extraction have imposed severe limitations, outweighing the benefits of enhanced charge separation. Hence integration of type II NRHs into PVs has thus far been unfruitful. Here, we demonstrate PVs that utilize NRHs as an extremely thin absorber between electron and hole transporting layers. In the limit approaching monolayer thickness, PVs incorporating NRHs have up to three times the short circuit current and conversion efficiency over devices made from their single-component counterparts. Comparisons between linear and curved NRHs are also made, revealing the importance of internal geometry and heterointerfacial area for enhanced contribution of charge-separated state absorption to photocurrent and in contacting charge transport layers.

KEYWORDS: nanocrystals · nanorods · heterostructures · photovoltaics · CdSe · CdTe

The performances of solar cells incorporating semiconductor nanocrystals (NCs) have dramatically improved in recent years with power conversion efficiencies exceeding 5% and absorbed photon-to-current-conversion efficiencies above 100% as new ways to utilize these quantum confined structures have been developed.[1,2] Improvements in efficiency combined with versatile solution processability (easy thin film formation at ambient conditions, incorporation into light-scattering and guiding media, *etc.*) make integration of NCs into next generation PVs very attractive.[3] Type II band offset nanocrystal heterostructures (NCHs) with epitaxial junctions between two different semiconductors exhibit additional advantages such as ultrafast photoinduced charge separation[4] and increased carrier lifetimes.[5,6] Type II NCHs can be synthesized in a variety of sizes and shapes with only minor modifications to the synthesis of single-component NCs. Anisotropic (noncore/shell) type II NCHs, nanorod heterostructures (NRHs) for example, are of particular interest because each component has exposed surface necessary for carrier extraction.[7] Anisotropic shape also provides directionality in guiding carriers. With strong absorption in the spectral range relevant to solar applications and well-established synthesis, CdSe/CdTe NRHs are especially promising PV materials.[8−10] The type II heterointerface leads to charge transfer or charge-separated state (CSS) absorption with a smaller binding energy penalty for dissociation and allows lower energy photons to be captured without sacrificing open circuit voltage (V_{oc}). Interfacial lattice strain can lead to further benefits.[11] For example, deposition of CdTe onto CdSe NR seeds could be easily varied from tip only growth of "linear" NRHs to partial side growth of highly strained "curved" NRHs,[12] providing additional means of tuning the band structure to manipulate photogenerated charges.

The built-in band offset, directionality in charge separation, and size/strain-tunable spectral response are salient features of CdSe/CdTe NRHs that could lead to significant performance advances in PVs. However, the ability of NRHs to improve PV performance has yet to be demonstrated because undesirable aspects such as surface charge traps and inefficient carrier transport, rather than advantages brought forth by the type II interface, can limit performance.[13−16] Hence, it is critical to identify the optimal role(s) of NRHs when integrating them into PVs. With the exception of quantum dot sensitized electrochemical solar cells, where incompatibility of most NCs with the corrosive electrolyte is a major roadblock,[17] previous applications of NCs in PVs used NCs as both a light absorber and a charge transport medium.[1,14,18] Charge transport through a NC film is quite inefficient due to the existence of surface traps and NC-NC hopping barriers[19−21] in addition to large charging energies.[22] Single-phase NCs may act as an effective absorber in polymer−NC (donor−acceptor) bulk heterojunction solar cells,[23] but once free

* Address correspondence to hmcdani2@illinois.edu; mshim@illinois.edu.

Received for review August 6, 2011 and accepted August 25, 2011.

Published online August 25, 2011
10.1021/nn2029988

carriers are created, electrons must find a pathway through interconnecting NCs to be extracted at the contact. Schottky junction solar cells incorporating NCs between conductors of differing work functions have been demonstrated as well[24] but again rely on inefficient transport of carriers through the NC film. Significant carrier mobilities and improved electrical conductivity have been observed in chemically treated (*via* ligand exchange)[20,25−28] and doped NC solids.[18,29] Therefore, substantial photocurrents can be observed in some of these NC solar cells where transport of only one type of carrier is required. However, the necessity of transport of both electrons and holes and the expected discontinuities in the conduction and valence bands that lead to carrier trapping[28] make transport inherently more difficult through a film of type II NRHs. Geyer *et al*. recently found that transport through films of CdSe/CdTe nanobarbells was dominated by hole transport and was nearly identical to transport through p-type films of CdTe NCs because it was dominated by interconnecting pathways of CdTe domains.[16] If CdSe/CdTe NRH films are to be used as absorbers in solar cells, both electrons and holes need to be transported (in opposite directions) through the film.

Hence the key question we seek to address here is how to exploit the advantages of a type II band offset in NRHs while circumventing problems of carrier transport. Through proof-of-concept PVs incorporating nanocrystal heterostructures (PINCHs), we demonstrate a 3-fold improvement in the overall conversion efficiency with CdSe/CdTe NRHs when compared to non-heterostructured single-component nanorod devices. The improvement arises from increases in both photovoltage and photocurrent. Enhanced CSS absorption in curved NRHs leads to further improvement in photocurrent. The active layer thickness dependence observed provides insights into improving PINCH device design.

PINCH: Type II NRHs As an Extremely Thin Absorbing Layer. In order to exploit efficient charge separation in type II NRHs without being limited by carrier transport and extraction, our solar cell design relies on a strategy similar to the extremely thin absorber (ETA) concept proposed by Kaiser *et al*.[30] In an ETA solar cell, two wide-gap semiconductors, forming a rectifying junction and having appropriate band energies, sandwich an "extremely" thin film of typically intrinsic absorbing material. Here, our PINCH devices are similar to ETA solar cells with type II NRHs, as the absorber. The key difference is that the NRHs with high-quality epitaxial heterointerfaces, also act as the charge separator, unlike ETA solar cells, where charge separation occurs at the often less well-defined absorber/wide gap semiconductor interface. In PINCHs, photogenerated electrons in NRHs are transferred to a wide-gap electron transport layer (ETL), while holes are transferred to a wide-gap hole transport layer (HTL). Both ETL and HTL

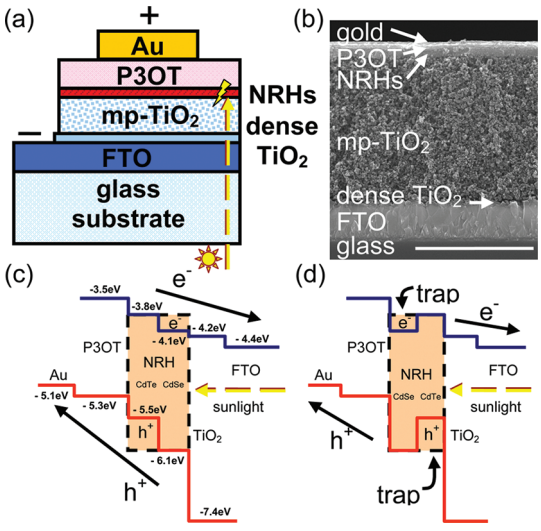

Figure 1. (a) Schematic of PINCH device structure. (b) SEM cross section of an actual device that contains four deposition cycles of linear NRHs for the absorbing layer. The scale bar is 2 μm. (c) Device band diagram for an ideally aligned NRH. Band edge positions are approximated based on reported band energies relative to vacuum level in addition to the optical band gaps experimentally measured *via* absorption spectra. (d) Band diagram for a NRH with a nonideal alignment.

should be chosen for high conductivity, photostability, and appropriate band energies to block minority carriers. This approach avoids exciton diffusion as the working principle, is expected to greatly improve exciton dissociation efficiencies, and does not require carrier transport through multiple NRHs.

As a proof-of-concept, we have fabricated devices with the layered structure depicted in Figure 1a. A scanning electron microscopy (SEM) image of the cross-section of a device is shown in Figure 1b. Four types of absorber layers, CdSe NRs, CdTe NRs, linear CdSe/CdTe NRHs, and curved CdSe/CdTe NRHs, have been compared. As seen in the approximate band diagram of a NRH device in Figure 1c, there is a clear driving force for electrons to migrate toward the fluorinated tin oxide (FTO) contact and for holes to head toward the Au contact. The ideal alignment is then for CdSe to contact TiO_2 (the ETL) and CdTe to contact poly(3-octylthiophene-2,5-diyl) (P3OT, the HTL). If a NRH is not appropriately aligned with the transport layers as shown in Figure 1d, the transport/blocking layers still prevent the NRH from acting like a shunt, but carriers may become trapped. We anticipate a combination of both types of band arrangements in our devices, where we expect the NRHs to be randomly oriented.

With the exception of devices fabricated to examine the layer thickness dependence discussed later, all devices consist of an absorber NR or NRH layer formed by a single deposition step from a solution (see Methods), resulting in approximately 40 nm in thickness (based on SEM imaging and estimated from optical density

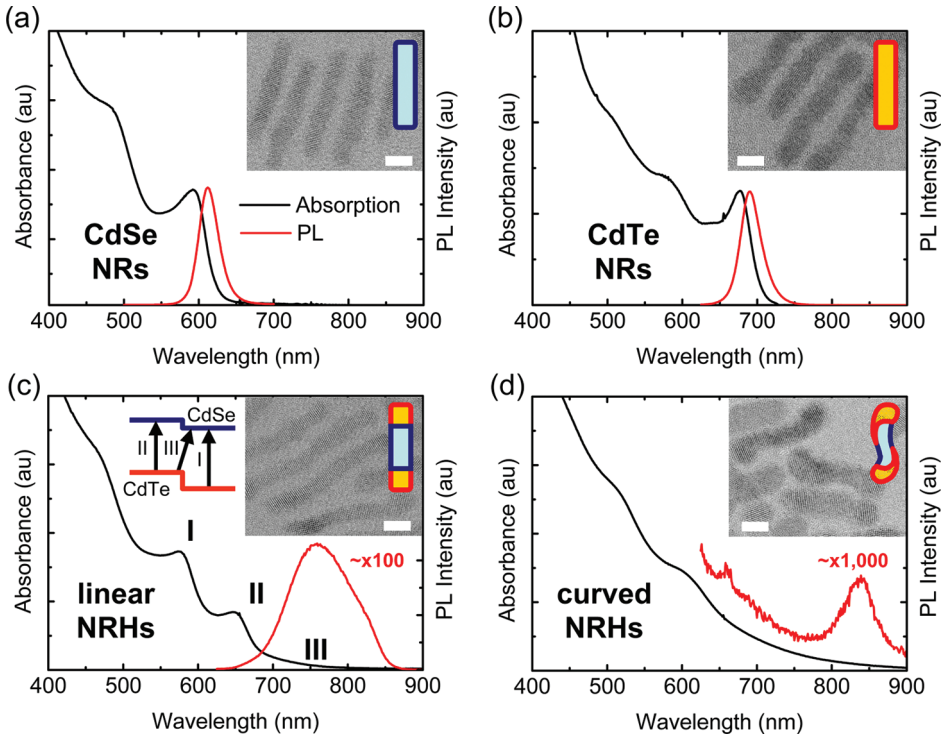

Figure 2. Absorption, photoluminescence, TEM image (inset), and structural schematic (inset) for the CdSe NRs (a), CdTe NRs (b), linear NRHs (c), and curved NRHs (d) used in this study. The scale bars of TEM images are 5 nm. Left inset in (c) shows optical transitions within the type II CdSe/CdTe band structure, which correspond to CdSe (I), CdTe (II), and CSS (III) absorption features.

using reported extinction coefficients[31]). Transmission electron microscopy (TEM) images of NRs and NRHs used in this study are shown in Figure 2a–d along with their absorption and photoluminescence (PL) spectra in solution. The syntheses are based on previous reports[8] in which CdSe or CdTe is grown epitaxially on seed CdSe NRs (or CdTe NRs for the CdTe only case) in a single pot (see Methods). The NRs and NRHs are recapped with pyridine and dissolved in a solution of methanol and pyridine for deposition onto device substrates.

The photocurrent action spectra (photocurrent relative to incident photons), also known as external quantum efficiency (EQE), of all four types of devices are plotted in Figure 3a–d. Features corresponding to exciton transitions are visible in the photocurrent, indicating that, through all device processing steps, quantum confinement is maintained. Absorption spectra of films of NRs and NRHs even after drying in a vacuum oven further confirm quantum confinement effects to be maintained (Supporting Figure S1). CdSe and CdTe NR control devices exhibit expected behavior in their photocurrent action spectra. The zero-bias photocurrent peak at the photon energy corresponding to the first exciton transition peak of CdTe is missing in both the CdTe NR control device and linear NRH device. These results are consistent with what has been observed in layered CdSe/CdTe NC PV cells previously reported.[16] This reduced contribution of direct CdTe excitation is likely caused by electron traps arising from CdTe surface oxidation which competes with the electron transfer across the heterointerface. Although the broad absorption feature near the CdTe first exciton transition makes it difficult to distinguish, we suspect the same effect is occurring in the curved NRH devices. These results indicate that photoexcitations that lead to both electrons and holes being generated in the CdTe region of NRHs are not very beneficial to PV performance. However, the key result is that devices incorporating curved NRHs exhibit significant photocurrent responses in the red tail of the spectrum which arises from CSS excitation at the heterointerface. Unlike the previous report of a layered device geometry consisting of CdSe NCs, linear CdSe/CdTe NRHs, and CdTe NCs,[16] photon energy absorbed directly into spatially separated excitons in our NRH devices do contribute significantly to the photocurrent, particularly in the case of the curved NRHs. The greater interfacial area leads to a larger CSS absorption cross section in the curved NRHs (Figure 2d) than in the linear NRHs (Figure 2c). The weakly bound electrons and holes in the CSS are more likely to be efficiently converted to free carriers that contribute to photocurrent. Further, large CSS absorption allows for low-energy photons (sub band gap of each component) to significantly contribute to photocurrent with minimal reduction in open circuit voltage, which is, in principle, determined by the band energies.

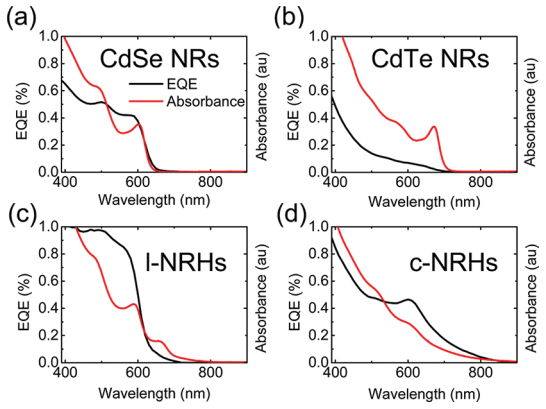

Figure 3. External quantum efficiency (EQE) of devices formed from single deposition cycle (~40 nm film) coating of recapped CdSe NRs (a), CdTe NRs (b), linear NRHs (c), and curved NRHs (d) and the corresponding as-synthesized solution absorption spectra.

***JV* Characteristics.** Having established that CSS transitions in NRHs can meaningfully contribute to PV performance in our PINCH devices, we compare current density *versus* voltage (*JV*) characteristics of the four devices under AM 1.5G simulated sunlight (100 mW/cm^2) in Figure 4. The devices exhibit good diode-like behavior in the dark, and all NR and NRH devices outperformed the control device consisting of a direct TiO_2/P3OT interface (Supporting Figure S2). The highest V_{oc} is observed in devices with linear NRHs (~0.60 V) followed by curved NRHs (~0.50 V), CdTe NRs (~0.40 V), and then CdSe NRs (~0.10 V). The maximum V_{oc} for these devices is set by the difference in the quasi-Fermi levels between the ETL and HTL. An upper limit for the quasi-Fermi level difference can be determined by the ETL (TiO_2) conduction band to HTL (P3OT) valence band offset, which is approximately 1.1 V. Less than the maximum possible V_{oc} reflects recombination processes present in the cell. The lowest V_{oc} observed in the CdSe NR control device may be explained by inefficient charge separation occurring at the CdSe NR/transport layer interfaces, which leads to greater recombination. Low short circuit current density (J_{sc}) in the CdTe NR device may be due to oxidation-induced electron traps. The higher V_{oc} in the CdTe NR device than the larger band gap CdSe NR device may be attributed to a larger driving force (conduction band offset) for electron transfer from CdTe to TiO_2,[32] thus reducing recombination. Devices incorporating NRHs, which are inherently good at charge separation, exhibit significantly better performance than the single-component NR control devices (higher V_{oc} and J_{SC}). The conversion efficiencies in the linear and the curved NRH devices are similar and roughly triple the CdTe devices. The improvement is even greater when compared with devices using CdSe NRs (7 times or better).

While the thinness of NRH films (only slightly thicker than the average length of individual NRHs) removes the necessity of inefficient transport through multiple NRHs, carrier extraction, especially electron extraction, may be expected to be problematic due to CdTe surface oxidation leading to electron traps.[16] Increased J_{sc} and V_{oc} in PINCH devices incorporating NRHs indicate that direct contact with transport layers can effectively compete with potential carrier trapping at the NRH surface. In particular, electron transfer to TiO_2 from NRHs should be more efficient than in single-component NR cases. In devices consisting of only CdSe NRs as the absorbing layer, surface oxidation induced electron traps are not as problematic, but charge separation, which should occur at the NR−transport layer interface, is expected to be less efficient due to interfacial recombination sites. Furthermore, charge transfer into the transport layer needs to overcome large exciton binding energies in CdSe NRs, whereas electrons are already separated from holes in type II NRHs. In CdTe NR only control devices, a similar exciton dissociation problem is also present. While surface oxide electron traps may enhance local charge separation, they would compete with electron transfer into TiO_2. In photoexcited NRHs, which have relaxed to the CSS, electrons are already separated from the holes and localized in CdSe (away from CdTe surface electron traps). Therefore, electron extraction into TiO_2 can compete effectively with trapping at the CdTe surface. Significantly higher J_{sc} in devices incorporating curved NRHs than in those with linear NRHs may be explained by the fact that curved structures absorb more strongly, especially in the red tail of the spectrum corresponding to the CSS transition.

While J_{sc} and V_{oc} both improve, NRH devices exhibit a somewhat unusual inflection point in their *JV* characteristics, which then leads to a lower fill factor. One explanation for the inflection point at ~0.3 V is that this is where the misaligned NRHs (*i.e.*, when CdSe and CdTe contact the wrong transport layers as shown schematically in Figure 1d) contribute to the PV response. At low biases (<0.3 V), misaligned NRHs do not contribute or contribute weakly to photocurrent due to charges being trapped within the NRHs (Figure 1d): CdSe-HTL and CdTe-ETL band offsets prevent carrier injection from transport layers into NRHs and therefore the subsequent recombination. When there is a large enough forward bias, charges in the transport layers can now overcome the barriers imposed by NRH-transport layer band offset and be injected into the misaligned NRHs, where they recombine and counter the photocurrent. Given that the conduction band offset between TiO_2 and CdTe is about 0.4 V, the inflection point appearing at ~0.3 V is consistent with a "threshold" external bias needed for electron injection from ETL into the misaligned NRHs, leading to recombination with photogenerated holes. Assuming random orientation, the chance for contact formation with the wrong transport layer should be about the same as the favorable contact formation in curved

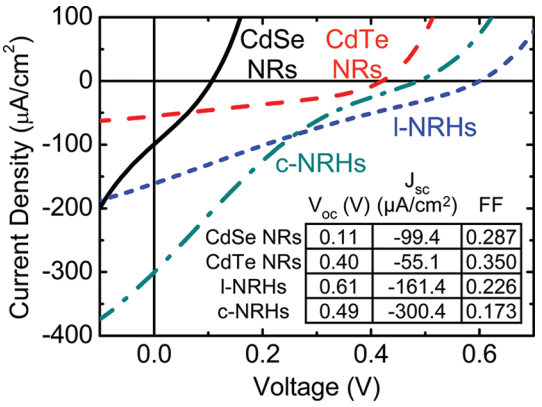

	V_{oc} (V)	J_{sc} (μA/cm²)	FF
CdSe NRs	0.11	-99.4	0.287
CdTe NRs	0.40	-55.1	0.350
l-NRHs	0.61	-161.4	0.226
c-NRHs	0.49	-300.4	0.173

Figure 4. Current density (*J*) *versus* voltage (*V*) characteristics for devices fabricated from one deposition cycle (~40 nm film) of recapped CdSe NRs, CdTe NRs, linear NRHs (l-NRHs), and curved NRHs (c-NRHs) under 100 mW/cm² AM 1.5G filtered light. The values of the open circuit voltage (V_{oc}), short circuit current (J_{sc}), and fill factor (FF) from each curve are shown in the inset.

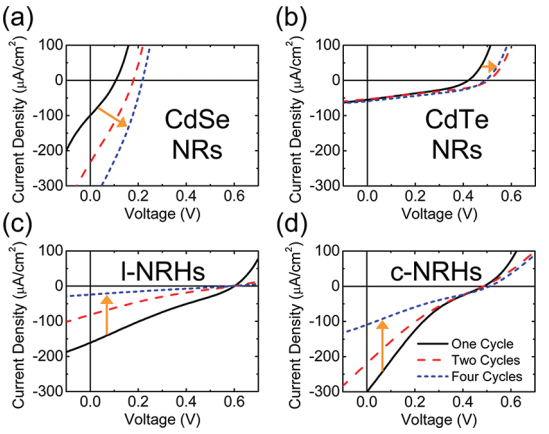

Figure 5. Absorber film thickness dependence of *JV* characteristics for devices fabricated with one, two, and four deposition cycles of CdSe NRs (a), CdTe NRs (b), linear NRHs (c), and curved NRHs (d), contrasting the effect of increasing absorbing layer thickness on performance of NR- *vs* NRH-based devices. The corresponding absorption spectra of these devices following each deposition cycle are shown in Supporting Figure S2.

NRHs, where a significant amount of CdTe deposits on the sides of the seed CdSe NRs. On the other hand, different orientations of linear NRHs with CdTe only at the tips (*i.e.*, more anisotropic shape) may lead to a larger number of distinct but less effective configurations in contacting the carrier transport layers, which in turn may make the inflection point in the *JV* characteristics less prominent at the expense of reduced photocurrent. Hence methods to properly align NRHs should lead to significant improvement in PV performance for both types of NRHs.

Divergent Effects of Increasing Film Thickness. In addition to improving NRH alignment, the amount of absorbing material can be optimized to enhance PV performance. Our current device design with a ~40 nm thick NR or NRH absorbing layer is only absorbing <10% of the incident light near the band edge transitions, which is far from optimal. The simplest approach to achieving more absorption is to increase the thickness of the absorbing layer. Additional NR/NRH deposition cycles lead to increasing absorbance (Supporting Figure S3), consistent with thickness increase observed by SEM (Supporting Figure S4) and a reduction in the dark current. For the devices incorporating single-component NRs, this additional thickness leads to more photons being absorbed, and the photocurrent increases as does the photovoltage (Figure 5a and b). These enhancements are more pronounced in CdSe NRs since surface oxidation of CdTe is expected to leave additional electron traps that counteract increased photon absorption.[16] Conversely, for both the curved and linear NRH PINCHs, additional deposition cycles lead to significantly reduced photocurrent, while the V_{oc} remains unchanged (Figure 5c and d). The decrease in photocurrent is consistent with the expectation that a thicker film of NRHs would lead to energy barriers for carrier transport, which reduces the number of carriers that can be extracted prior to recombination. Note that the thickness of ~40 nm arising from a single deposition cycle is only slightly larger than the average length of the NRHs (~33 nm). The reduction in photocurrent with NRH film thickness emphasizes the importance of having both the ETL and HTL in close proximity to (in contact with) an absorbing NRH for extracting photocurrent, *i.e.*, to avoid transport through multiple NRHs where type II band offset related traps (in addition to surface traps) can make transport highly inefficient.

CONCLUSIONS

Many studies of type II NRHs have been motivated by solar energy applications, yet few have actually incorporated these structures into devices[13,15,16] and none have demonstrated an improvement over single-component NR-based devices. With our relatively simple device design, we have shown that CSS transitions arising from type II band offset in NRHs can contribute substantially to PV performance improvement. Our results also point to areas for improvement in device design. The thickness effects indicate that in order to exploit type II NRHs in solar cells, they need to serve as absorbers but not as charge transport media. Lower FFs, most likely arising from NRHs being misaligned with transport layers, suggest the need for improvement in the NRH deposition process to maximize contact between the CdSe (CdTe) component and ETL (HTL). Interestingly, curved NRHs with a significant amount of CdTe grown on the sides of CdSe seed NRs exhibit better performance than the linear NRHs when deposited randomly. Since our current device design does not fully utilize incident photons, increasing the number of NRHs in the absorption layer is necessary. This increase should be achieved by conformally

coating a high surface area ETL (or HTL) and infilling with the HTL (or ETL) to avoid problems of carrier transport through multiple NRHs. Given that NRHs do not substantially penetrate a mesoporous TiO_2 ETL of ~25 nm average diameter, simply increasing the TiO_2 pore size may lead to a significant improvement.

Optimizing the internal structure of individual NRHs to promote CSS absorption can also greatly enhance PV performance. Nearly a factor 2 larger J_{sc} observed in curved NRH devices (over the linear NRH devices) is indicative of this importance. In addition to the increasing heterointerface area and improving NRH morphology to optimize proper contact with ETL and HTL, lattice strain within NRHs may also be an important factor. For example, highly strained curved NRHs exhibit much lower PL efficiency than linear NRHs (Figure 2), which may arise from enhanced and long-lived charge separation (and thereby reduced radiative recombination) due to band offset/band structure modification by interfacial strain. Further work is needed to understand carrier dynamics in such strained NRHs to determine what role(s) strain might play in charge separation and extraction.

METHODS

Synthesis of NRs and NRHs. The single-pot syntheses are based on previous reports,[8,12] and the details can be found in the Supporting Information. Briefly, CdSe seeds (for CdSe NRs, linear NRHs, and curved NRHs) and CdTe seeds (for CdTe NRs) were formed by swiftly injecting TOP-(Se or Te) into a degassed solution of TOPO and ODPA-Cd at 320 °C (TOP = trioctylphosphine, TOPO = trioctylphosphine oxide, and ODPA = octadecyl phosphonic acid). Upon injection, the temperature was rapidly quenched to 260 °C, where the seeds were grown. After growing the seed NRs for 20 min, TOP-(Se,Te) was slowly injected via a syringe pump over 15 min to extend the growth of NRs further or to form the second component of the linear NRHs. For curved NRHs, TOP-Se was injected at 300 °C. The NRs and NRHs were then cleaned twice by dissolution in chloroform and precipitation with a butanol/methanol solvent mixture to remove any excess OPDA, ODPA-Cd, and TOPO. Finally, the NRs and NRHs were recapped with pyridine.

Device Fabrication. FTO-coated glass substrates were cut into 2 cm × 1.1 cm pieces, then cleaned by sonication in acetone and rinsed with DI water and 2-propanol. Dense TiO_2 (200 nm) was deposited onto the substrates at 400 °C by spray pyrolysis (8.58 mL of ethanol, 0.82 mL of acetylacetone, and 0.59 mL of titanium(IV) isopropoxide per substrate). The dense TiO_2 was removed from one edge of the FTO/glass substrate with a razor blade to expose the back contact. A ~1.5 μm thick layer of mesoporous TiO_2 (Dyesol paste) was screen printed with a 90T mesh and sintered at 500 °C in air with the following heat treatment: room temperature to 500 °C at a rate of 3 °C/min, held at 500 °C for 1 h, then 500 °C to room temperature at a rate of −5 °C/min. The heat-treated substrates were dipped into pyridine recapped NR or NRH solutions (see Supporting Information) and dried with N_2 flow after excess solution was wicked away with a paper wipe to produce a film that was optically homogeneous. We define this procedure to deposit NR or NRH film from solution as one deposition cycle. For thicker films, additional deposition cycles were carried out as indicated. After NR or NRH film deposition, a ~30 nm film of P3OT was then spin coated at 2000 rpm in air from a prepared solution of 34 mg of P3OT in 0.29 g of chloroform and 12.6 g of xylenes. The devices were then baked in a vacuum oven (~100 Torr) at 100 °C for 24 h. A 100 nm Au top contact was deposited by electron beam evaporation at 0.5 Å/s at 5×10^{-6} Torr using a shadow mask. The active area of each device was 0.283 cm^2.

Characterization. Transmission electron microscopy samples were prepared on Cu grids with a thin carbon film from a dilute solution of NCs in chloroform. TEM analysis was carried out with a JEOL 2100 TEM operating at 200 kV. HRTEM and STEM analyses were carried out with a JEOL 2200 aberration-corrected STEM/TEM operating at 200 kV. SEM images were taken with a Hitachi S-4800 at 10 kV. Cross sections were prepared from samples using a glass cutter; then Pd/Au was sputtered onto the cross section to reduce charging. UV−vis absorption spectra were obtained with an Agilent 8453 photodiode array spectrometer. Photoluminescence spectra were collected with a Horiba Jobin Yvon FluoroMax-3 fluorometer. Dark and light *JV* curves were measured immediately after device fabrication using a Keithly 2400 source meter. The measurements were taken at 0.01 V/step, 1 s/step. Simulated sunlight at 100 mW/cm^2 was generated by a Newport solar simulator with an AM 1.5G filter. External quantum efficiency was measured with an OL 750 spectroradiometer under a light bias. Measurements were taken in steps of 10 nm with a 1−2 s delay between steps. The chopper frequency was set to 41 Hz.

Acknowledgment. The authors thank Prof. Lane Martin for use of the solar simulator and Julio Soares for assistance with quantum efficiency measurements. This material is based upon work supported in part by the NSF (Grant No. 09-05175) and UIUC. Experiments were carried out in part in the Frederick Seitz Materials Research Laboratory Central Facilities, University of Illinois.

Supporting Information Available: Effect of vacuum oven treatment on film absorbance, dark *JV* for single dip devices, TiO_2/P3OT (no NRs or NRHs) light *JV*, thickness effect on film optical density, SEM on cross sections of devices with increasing thickness, and details of NR and NRH synthesis. This material is available free of charge *via* the Internet at http://pubs.acs.org.

REFERENCES AND NOTES

1. Pattantyus, A. G.; Kramer, I. J.; Barkhouse, A. R.; Wang, X.; Konstantatos, G.; Debnath, R.; Levina, L.; Raabe, I.; Nazeeruddin, M. K.; Grätzel, M.; Sargent, E. H. Depleted-Heterojunction Colloidal Quantum Dot Solar Cells. *ACS Nano* **2010**, *4*, 3374–3380.
2. Sambur, J. B.; Novet, T.; Parkinson, B. A. Multiple Exciton Collection in a Sensitized Photovoltaic System. *Science* **2010**, *330*, 63–66.
3. Gur, I.; Fromer, N. A.; Geier, M. L.; Alivisatos, A. P. Air-Stable All-Inorganic Nanocrystal Solar Cells Processed from Solution. *Science* **2005**, *310*, 462–465.
4. Dooley, C. J.; Dimitrov, S. D.; Fiebig, T. Ultrafast Electron Transfer Dynamics in CdSe/CdTe Donor-Acceptor Nanorods. *J. Phys. Chem. C Lett.* **2008**, *112*, 12074–12076.
5. Chuang, C.; Lo, S. S.; Scholes, G. D.; Burda, C. Charge Separation and Recombination in CdTe/CdSe Core/Shell Nanocrystals as a Function of Shell Coverage: Probing the Onset of the Quasi Type-II Regime. *J. Phys. Chem. Lett.* **2010**, *1*, 2530–2535.
6. Lee, D. C.; Robel, I.; Pietryga, J. M.; Klimov, V. I. Infrared-Active Heterostructured Nanocrystals with Ultralong Carrier Lifetimes. *J. Am. Chem. Soc.* **2010**, *132*, 9960–9962.
7. Bang, J.; Park, J.; Lee, J. H.; Won, N.; Nam, J.; Lim, J.; Chang, B. Y.; Lee, H. J.; Chon, B.; Shin, J.; *et al.* ZnTe/ZnSe (Core/Shell) Type-II Quantum Dots: Their Optical and Photovoltaic Properties. *Chem. Mater.* **2010**, *22*, 233–240.
8. Shieh, F.; Saunders, A. E.; Korgel, B. A. General Shape Control of Colloidal CdS, CdSe, CdTe Quantum Rods and

Quantum Rod Heterostructures. *J. Phys. Chem. B Lett.* **2005**, *109*, 8538–8542.
9. Halpert, J. E.; Porter, V. J.; Zimmer, J. P.; Bawendi, M. G. Synthesis of CdSe/CdTe Nanobarbells. *J. Am. Chem. Soc.* **2006**, *128*, 12590–12591.
10. Kumar, S.; Jones, M.; Lo, S. S.; Scholes, G. D. Nanorod Heterostructures Showing Photoinduced Charge Separation. *Small* **2007**, *3*, 1633–1639.
11. Smith, A. M.; Mohs, A. M.; Nie, S. Tuning the Optical and Electronic Properties of Colloidal Nanocrystals by Lattice Strain. *Nat. Nanotechnol.* **2008**, *4*, 56–63.
12. McDaniel, H.; Zuo, J. M.; Shim, M. Anisotropic Strain Induced Curvature in Type II CdSe/CdTe Nanorod Heterostructures. *J. Am. Chem. Soc.* **2010**, *132*, 3286–3288.
13. Zhong, H.; Zhou, Y.; Yang, C.; Li, Y. Synthesis of Type II CdTe-CdSe Nanocrystal Heterostructured Multiple-Branched Rods and Their Photovoltaic Applications. *J. Phys. Chem. C* **2007**, *111*, 6538–6543.
14. Li, B. Y.; Mastria, R.; Fiore, A.; Nobile, C.; Yin, L. X.; Biasiucci, M.; Cheng, G.; Cucolo, A. M.; Cingolani, R.; Manna, L.; Gigli, G. Improved Photovoltaic Performance of Heterostructured Tetrapod-Shaped CdSe/CdTe Nanocrystals Using C60 Interlayer. *Adv. Mater.* **2009**, *21*, 4461–4466.
15. Rivest, J. B.; Swisher, S. L.; Fong, L.-K.; Zheng, H.; Alivisatos, A. P. Assembled Monolayer Nanorod Heterojunctions. *ACS Nano* **2011**, *5*, 3811–3816.
16. Geyer, S.; Porter, V. J.; Halpert, J. E.; Mentzel, T. S.; Kastner, M. A.; Bawendi, M. G. Charge Transport in Mixed CdSe and CdTe Colloidal Nanocrystal Films. *Phys Rev. B* **2010**, *82*, 1552011–1552018.
17. Bang, J. H.; Kamat, P. V. Quantum Dot Sensitized Solar Cells. A Tale of Two Semiconductor Nanocrystals: CdSe and CdTe. *ACS Nano* **2009**, *3*, 1467–1476.
18. Sun, B.; Findikoglu, A. T.; Sykora, M.; Werder, D. J.; Klimov, V. I. Hybrid Photovoltaics Based on Semiconductor Nanocrystals and Amorphous Silicon. *Nano Lett.* **2009**, *9*, 1234–1241.
19. Yu, D.; Wang, C.; Guyot-Sionnest, P. n-Type Conducting CdSe Nanocrystal Solids. *Science* **2003**, *300*, 1277–1280.
20. Vanmaekelbergh, D.; Liljeroth, P. Electron-Conducting Quantum Dot Solids: Novel Materials Based on Colloidal Semiconductor Nanocrystals. *Chem. Soc. Rev.* **2005**, *34*, 299–312.
21. Liu, Y.; Gibbs, M.; Puthussery, J.; Gaik, S.; Ihly, R.; Hillhouse, H. W.; Law, M. Dependences of Carrier Mobility on Nanocrystal Size and Ligand Length in PbSe Nanocrystals Solids. *Nano Lett.* **2010**, *10*, 1960–1969.
22. Shim, M.; Guyot-Sionnest, P. Permanent Dipole Moment and Charges in Colloidal Semiconductor Quantum Dots. *J. Chem. Phys.* **1999**, *111*, 6955–6964.
23. Huynh, W. U.; Dittmer, J. D.; Alivisatos, A. P. Hybrid Nanorod-Polymer Solar Cells. *Science* **2002**, *295*, 2425–2427.
24. Luther, J. M.; Law, M.; Beard, M. C.; Song, Q.; Reese, M. O.; Ellingson, R. J.; Nozik, A. J. Schottky Solar Cells Based on Colloidal Nanocrystal Films. *Nano Lett.* **2008**, *8*, 3488–3492.
25. Talapin, D.; Murray, C. B. PbSe Nanocrystal Solids for n- and p-Channel Field-Effect Transistors. *Science* **2005**, *310*, 86–89.
26. Konstantatos, G.; Howard, I.; Fischer, A.; Hoogland, S.; Clifford, J.; Klem, E.; Levina, L.; Sargent, E. H. Ultrasensitive Solution-Cast Quantum Dot Photodetectors. *Nature* **2006**, *442*, 180–183.
27. Murphy, J. E.; Beard, M. C.; Nozik, A. J. Time-Resolved Photoconductivity of PbSe Nanocrystal Arrays. *J. Phys. Chem. B* **2006**, *110*, 25455–25461.
28. Lee, J.-S.; Kovalenko, M. V.; Huang, J.; Cheng, D. S.; Talapin, D. V. Band-like Transport, High Electron Mobility and High Photoconductivity in All-Inorganic Nanocrystal Arrays. *Nat. Nanotechnol.* **2011**, *6*, 348–352.
29. Wehrenberg, B. L.; Yu, D.; Ma, J.; Guyot-Sionnest, P. Conduction in Charged PbSe Nanocrystal Films. *J. Phys. Chem. B* **2005**, *109*, 20192–20199.
30. Kaiser, I.; Ernst, K.; Fischer, C. H.; Konenkamp, R.; Rost, C.; Sieber, I.; Lux-Steiner, M. C. The ETA-Solar Cell with $CuInS_2$: A Photovoltaic Cell Concept Using an Extremely Thin Absorber (ETA). *Sol. Energy Mater. Sol. Cells* **2001**, *67*, 89–96.
31. Yu, W. W.; Qu, L.; Guo, W.; Peng, X. Experimental Determination of the Extinction Coefficient of CdTe, CdSe, and CdS Nanocrystals. *Chem. Mater.* **2003**, *15*, 2854–2860.
32. Robel, I.; Kuno, M.; Kamat, P. V. Size-Dependent Electron Injection from Excited CdSe Quantum Dots into TiO_2 Nanoparticles. *J. Am. Chem. Soc.* **2007**, *129*, 4136–4137.